Defence Technology 13 (2017) 143–149

Contents lists available at ScienceDirect

Defence Technology

journal homepage: www.elsevier.com/locate/dt

Impact-disrupted gunshot residue: A sub-micron analysis using a novel collection protocol

V. Spathis

School of Physical Sciences, University of Kent, Canterbury, Kent CT2 7NZ, United Kingdom

ARTICLE INFO

Article history:
Received 30 January 2017
Received in revised form
19 March 2017
Accepted 29 March 2017
Available online 4 May 2017

Keywords:
Gunshot residue
Impact-disrupted gunshot residue
Sub-micron
Scanning electron microscopy
Cold field emission SEM
FEG-SEM
X-flash
Energy dispersive X-ray spectrometry

ABSTRACT

The analysis of gunshot residue (GSR) has played an integral role within the legal system in relation to shooting cases. With a characteristic elemental composition of lead, antimony, barium, and a typically discriminative spheroidal morphology, the presence and distribution of GSR can aid in firearm investigations. In this experiment, three shots of low velocity rim-fire ammunition were fired over polished silicon collection substrates placed at six intervals over a 100 cm range. The samples were analysed using a Field Emission Gun Scanning Electron Microscope (FEG-SEM) in conjunction with an *X-flash* Energy Dispersive X-ray (EDX) detector, allowing for GSR particle analyses of composition and structure at the sub-micron level. The results of this experiment indicate that although classic spheroidal particles are present consistently throughout the entire range of samples their sizes vary significantly, and at certain distances from the firearm particles with an irregular morphology were discerned, forming "impact-disrupted" GSR particles, henceforth colloquially referred to as "splats". Upon further analysis, trends with regards to the formation of these splat particles were distinguished. An increase in splat frequency was observed starting at 10 cm from the firearm, with 147 mm^{-2} splat density, reaching a maximal flux at 40 cm (451 mm^{-2}), followed by a gradual decrease to the maximum range sampled. Moreover, the structural morphology of the splats changes throughout the sampling range. At the distances closest to the firearm, molten-looking particles were formed, demonstrating the metallic residues were in a liquid state when their flight path was disrupted. However, at increased distances-primarily where the discharge plume was at maximum dispersion and moving away from the firearm, the residues have had time to cool in-fight resulting in semi-congealed and solid particles that subsequently disrupted upon impact, forming more structured as well as disaggregated splats. The relative compositions of the characteristic elements that are present in GSR also change in the different splat morphologies sampled, which may contribute to the particles' physical structures. Two distinct populations of splats were also observed: circular and elongated, which suggest the residues hit the substrate at different angles. The difference in the splat impact angle can be ascribed to the position of the residues within the firearm discharge plume; particles get caught up in the vortex that is created by the discharge gases behind the projectile as it leaves the barrel, thereby affecting their directionality and flight time. This reasoning could also justify the existence of both spheroidal and splat particles at certain distances. The novel sampling and analytical techniques used in this experiment have provided previously unknown information in relation to GSR structure and formation which could have greater implications to its current analysis amongst laboratories and law enforcement agencies worldwide.

1. Introduction

When a cartridge-based weapon is fired, both gaseous and solid residues consisting of organic and inorganic particles from the ammunition are produced and expelled from the barrel [1–3]. Once these residues are in flight they cool very rapidly producing GSR, which is identified by its characteristic inorganic elemental composition of lead, antimony and barium [4]. The analysis of GSR provides important evidence in firearms incidents, making the quality of its analysis crucial. Therefore, it was established that SEM-EDX analysis was the ideal technique to do so due to its non-destructive ability to analyse samples and being able to provide

E-mail address: v.spathi@kent.ac.uk.
Peer review under responsibility of China Ordnance Society.

http://dx.doi.org/10.1016/j.dt.2017.03.007

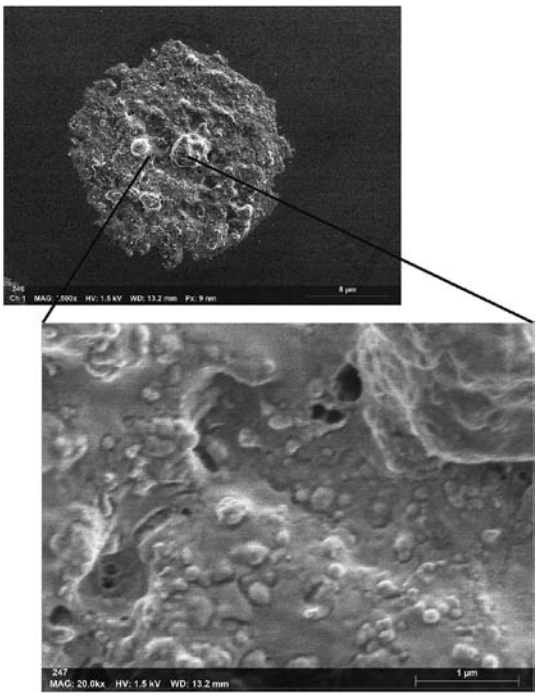

Fig. 1. FEG-SEM image of impact-disrupted GSR showing the imaging capabilities of a cold field emission SEM. Scale on zoomed in image: 1 µm *HV 1.5 kV.*

morphological and elemental composition data in a short amount of time [5,6]. Although GSR has a characteristic elemental composition, the origin of those particles cannot be concluded based on that alone. It has been acknowledged that to establish a particle is in fact GSR, the compositional data must be coupled with a characteristic spheroidal morphology to distinguish it from environmental aggregates such as residue from fireworks or vehicle brake pads [7–11]. In this experiment, the morphology and elemental composition of rimfire ammunition GSR is examined. Although the concept of coalescence of molten droplets to form GSR is not unknown [12] the novel sampling and analytical techniques used in this experiment demonstrate that particles may not always have sufficient time to cool into spheroidal residues, in particular at low velocities.

2. Materials and method

2.1. Experimental setup

In this experiment, six silicon collection substrates sized approximately 15 mm × 20 mm were set up perpendicular to the firearm and 7 cm below the firing line at bench level. The collection substrates were kept upright and in place with the use of plastic spine bars that were fixed onto the bench, allowing the substrates to be at a consistent height and perpendicular to the firearm for maximum residue collection. Prior to the experiment, these silicon substrates were cleaned for 5min in an ultrasonic bath using HPLC

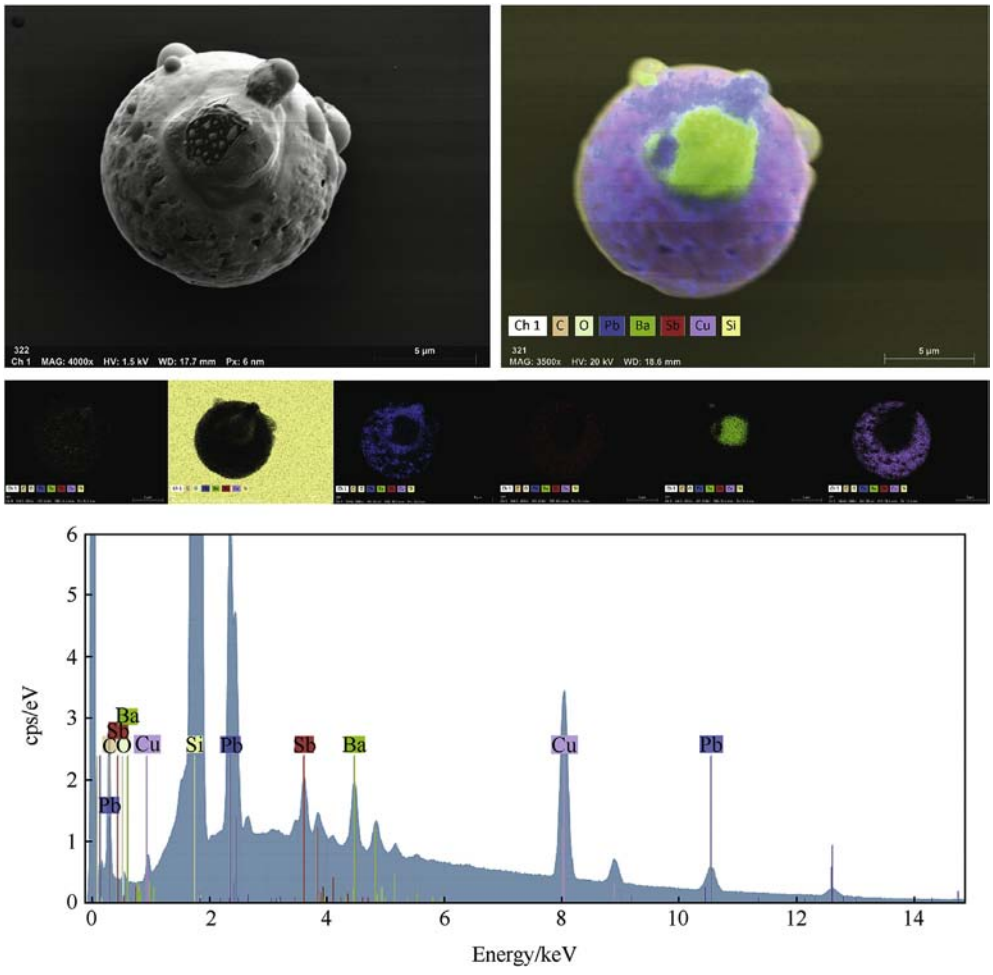

Fig. 2. FEG-SEM/EDX image of a characteristic spherical GSR showing sub-micron elemental distribution using the Bruker *X-flash* 5060f flat quad EDX detector. Image: *HV 1.5 kV.*, Elemental maps: *HV 20 kV.*

grade acetone and left to dry, placed in their individual containers and were only taken out for the test firing in a closed room using gloves. This ensured that they remained as uncontaminated as possible, and residues found on them during the analytical process were a product of the firing and not prior contaminants. These substrates were arranged in a straight line down the centre of the firing line at distances of 10 cm, 20 cm, 40 cm, 60 cm, 80 cm and 100 cm. Three consecutive shots were fired using 0.22″ 376 m s^{-1} CCI Minimag full metal jacketed (FMJ) rimfire ammunition with a Browning Buckmark long rifle pistol.

2.2. Analytical method

The silicon samples were collected immediately after the test firing and mounted on double sided carbon adhesive tape on aluminium stubs, allowing for SEM analysis. They were then analysed using a Hitachi S-4700 cold field emission SEM equipped with a Bruker *X-flash* 5060f flat quad energy dispersive X-ray detector [13], which allowed for the examination of particle structural morphology (Fig. 1) and elemental composition (Fig. 2) at the submicron level. The morphology of the particles was examined using an accelerating voltage of 1.5 kV, which provided a more elaborate insight into the surface topography of a particle as the electron beam does not penetrate deep into the sample [14]. However, during the elemental composition acquisition process, the voltage was changed to 20 kV. This gave a poorer image of the particle (as the electron beam is more penetrating and thus surface features are rendered invisible) but the higher accelerating voltage is required to stimulate X-ray emission from metallic elements comprising the particle.

3. Results

Upon FEG-SEM analysis of the samples, it appeared that the frequency at which particles were present on each silicon substrate varied significantly. It was determined that the majority of the residues collected had an irregular morphology rather than their frequently encountered spheroidal shape. This was done by setting up a 'Particle Mapping Job' on the FEG-SEM using the Bruker Esprit software which allowed for image and X-ray data to be acquired over a customisable area. Approximately half the surface area of the sample was analysed using this automated method at 20 kV. The results were then reviewed and the particles were then manually examined, as well as the rest of the sample, using a random selection process. Within these particles, there were two populations distinguished, normal incidence and angled splats (Fig. 3). Consequent to further analysis, this selection of particles could be divided further into several subcategories (Fig. 4 and Fig. 5).

A class of particles shown in Fig. 6 was also encountered throughout all of the samples. However, as they primarily consisted of organic material with only small amounts of the inorganic 'characteristic' GSR elements, they were excluded from the classification process. The silicon substrates were analysed and a random selection of particles was chosen from each. These particles were then classified using the splat classification diagram and archetypes mentioned in Figs. 4 and 5. The results are displayed in Table 1.

A selection of splats from each class was analysed using EDX (Fig. 7). The elemental data was collated and is displayed in Table 2. The relative proportions of the 'characteristic' GSR elements in each class was also plotted to show elemental composition change per classification type (Fig. 8).

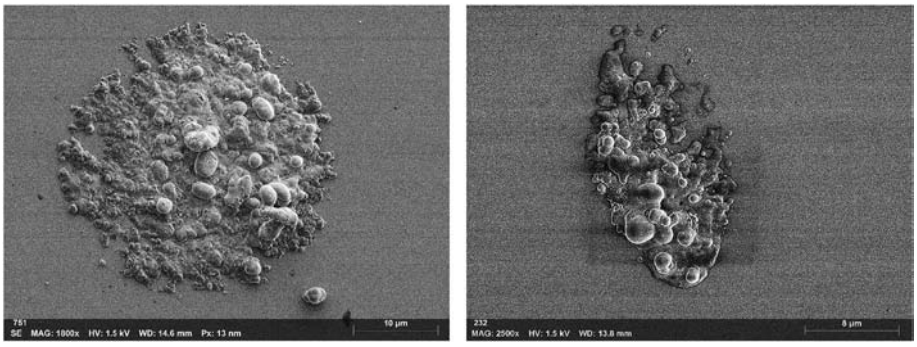

Fig. 3. FEG-SEM images of two different impact disrupted GSR populations. Left: normal incidence splat. Right: angled splat. *HV 1.5 kV.*

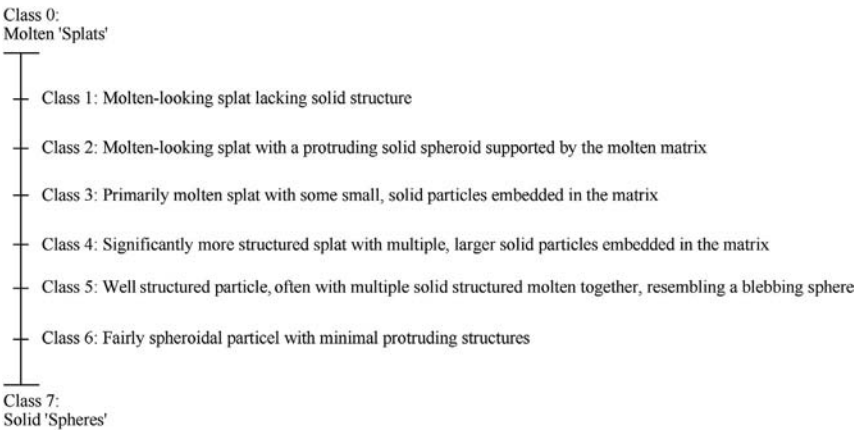

Fig. 4. Diagram describing the different splat classifications.

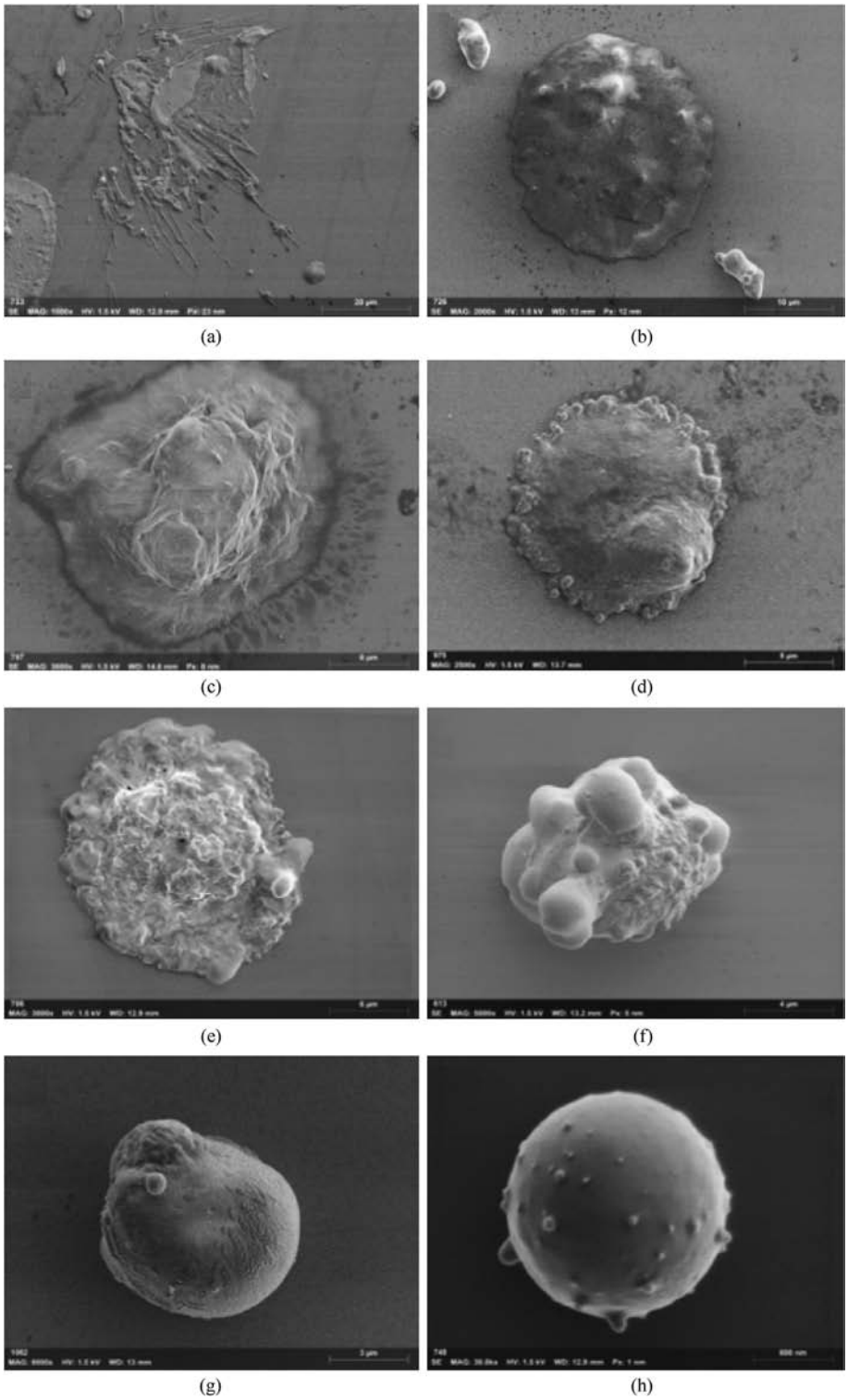

Fig. 5. FEG-SEM images of archetype impact-disrupted GSR populations over 100 cm range. A: Class 0, B: Class 1, C: Class 2, D: Class 3, E: Class 4, F: Class 5, G: Class 6, H: Class 7. *HV 1.5 kV.*

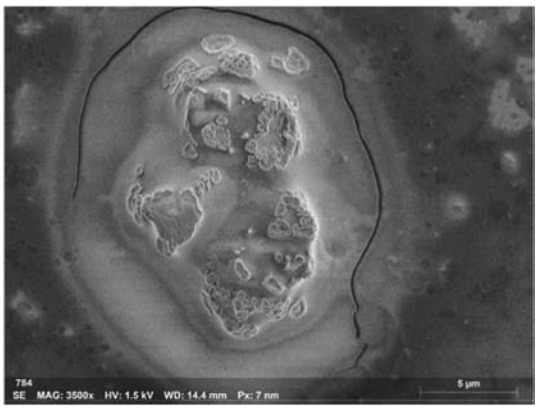

Fig. 6. FEG-SEM image of a primarily organic particle with some inorganic elements.

different temperature or velocity. As is demonstrated in Fig. 9, when the projectile leaves the barrel, it creates an expanding vortex behind it. The vortex keeps expanding until it reaches maximum dispersion, after which it starts to diminish. However, although the particles get trapped in that vortex, the majority of them still do not have sufficient time to cool despite the increased flight time. This suggests that the residues found at these distances are either experiencing a higher temperature effect or are travelling at a higher velocity than the particles found closer to the firearm. The travelling of particles in the firearm discharge plume is also responsible for the different splat angles seen in Fig. 3 in section 3. Although some particles maintain a fairly straight flight path resulting in normal incidence splats, others get trapped in the vortex that is created, resulting in a change in their directionality, and therefore impacting the substrate at an angle. Moreover, the spherical particles that were found at these distances were smaller

Table 1
Table showing the number of particles per silicon substrate and their corresponding classifications.

Silicon substrate number	Distance from firearm/cm	Number of particles per class/%								Total number of particles examined
		0	1	2	3	4	5	6	7	
1	10	0.9	1.7	41.9	0.9	0.0	35.9	12.0	0.9	117
2	20	0.0	7.5	40.0	13.3	4.2	22.5	10.0	0.0	120
3	40	2.7	50.0	4.0	17.3	9.3	8.7	0.7	4.7	150
4	60	2.9	5.9	3.9	24.5	23.5	23.5	9.8	2.9	102
5	80	0	2.5	0.8	13.9	22.1	35.2	21.3	4.1	122
6	100	0	0	8.9	3.6	12.5	50.9	10.7	8.0	112

Although copper does not come under the ASTM guide for characteristic GSR elements, it was present in the vast majority of particles analysed (in conjunction with Pb, Sb and Ba) and was therefore included to ensure more accurate relative particle compositions.

4. Discussion

4.1. Morphological analysis

The results from the morphological examination of the impact disrupted GSR indicate that there is a clear pattern in class type as a function of distance. As it can be seen from Table 1, at the distances closest to the firearm a high number of class 2 and class 5 particles are observed, with minor contributions to the other classes. However, around the centre of the sampling range, at approximately 40 cm from the firearm, the residues analysed primarily fall within classes 1, 3 and 4. Here, the firearm discharge plume is at its maximum dispersion for this specific firearm and ammunition combination. This was established by having previously carried out a test firing with the same firearm and ammunition combination where a 25 cm × 25 cm piece of cotton fabric was set up at 10 cm intervals from the firearm up to a maximum of 100 cm. A single shot was fired through each piece of fabric and the Modified Griess and Sodium Rhodizonate tests were carried out to reveal the nitrite and lead residue dispersion pattern on the fabric [15]. These data suggest that although these residues appear further away from the firearm, they have not had sufficient time to cool in-flight, resulting in their liquid and molten forms. This is contradicted by the fact that residues closer to the firearm inhabit a more solid structure despite being only 10 cm or 20 cm away. Therefore, this exhibits that there are two different directionalities to the firearm discharge plume, each of which may be subject to a than 3 µm. This information supports the aforementioned hypothesis as small, spheroidal particles would have had the chance to cool because of their small volume. To first order, the relative particle cooling time is a function of the volume of a particle, and thus is 8 times faster for a particle with half the diameter. On the other hand, the larger particles would not have had the chance to cool because of their added size, resulting in their disruption upon impact. In consequence, this means that the residues found closer to the firearm are present as a result of the lower velocity stream of particles that leaves the muzzle, labelled 'A'. This is reinforced by the fact that at the distances farthest from the firearm, there is a gradual increase in more semi-congealed and solidified residues, as well as the characteristic spherical GSR.

4.2. Elemental composition analysis

Upon examination of the elemental composition of the different particle classes, it can be seen that the more liquid the appearance of the particle, the higher the lead content of said particle appears to be. Conversely, as it can be seen in Fig. 8 in section 4.2, the barium content seems to increase as the particles become more solidified. Antimony and copper both show a slight decrease as the residues become more structured and solid. However, as multiple particles throughout the sampling range were analysed, it appeared that these particles are fairly antimony-poor and upon EDX analysis of the cartridge case, projectile and primer, it was determined the ammunition itself contained no antimony. In fact, the presence of antimony in the samples was due to the projectile itself. Some anomalous particles have influenced these results, leading to larger than average error. Nevertheless, a change in the compositional ratios in these particles could influence their structural morphology, therefore, suggesting that the ratio of the elemental composition may also influence a particle's structure, in

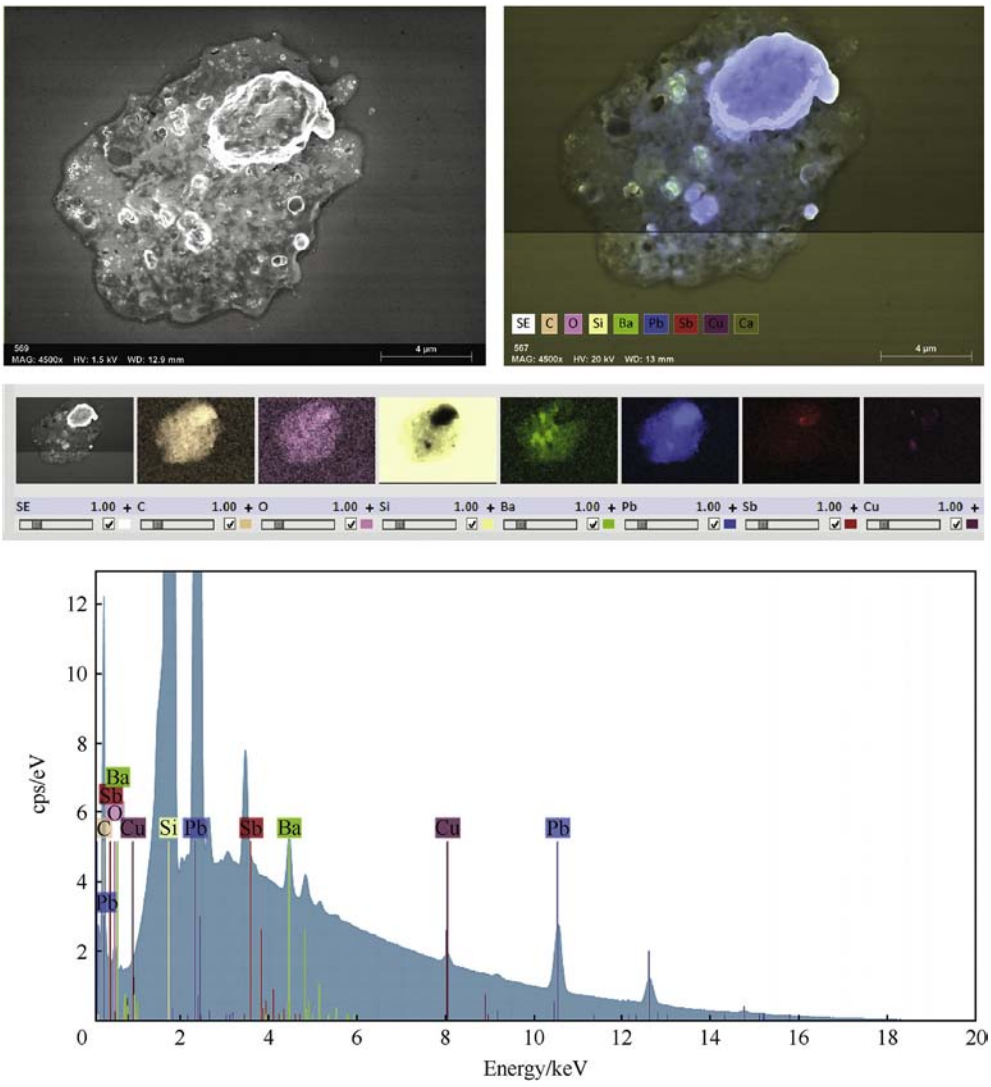

Fig. 7. FEG-SEM/EDX image of an impact disrupted GSR particle showing sub-micron elemental distribution using the Bruker *X-flash* 5060f flat quad EDX detector. Image: *HV 1.5 kV.*, Elemental maps: *HV 20 kV.*

Table 2
Table showing the relative proportions of 'characteristic' elements present in GSR ± 1 standard deviation.

Class number	Relative particle compositions of 'characteristic' gsr elements/%			
	Pb	Sb	Ba	Cu*
0	78.26 ± 6.33	4.92 ± 0.70	7.70 ± 5.42	9.12 ± 0.60
1	83.03 ± 3.85	2.71 ± 0.91	9.81 ± 3.02	4.44 ± 1.50
2	88.44 ± 2.51	4.30 ± 0.89	3.48 ± 1.54	3.78 ± 1.33
3	82.83 ± 3.17	2.87 ± 1.90	10.87 ± 3.02	3.43 ± 0.78
4	84.65 ± 3.84	2.62 ± 0.68	8.73 ± 1.73	4.01 ± 1.89
5	80.55 ± 21.60	1.79 ± 0.60	13.97 ± 21.99	3.69 ± 0.94
6	75.72 ± 35.96	2.02 ± 0.98	18.53 ± 37.60	3.73 ± 1.76
7	78.11 ± 32.84	2.90 ± 1.89	16.90 ± 33.23	2.09 ± 1.13

conjunction with in-flight cooling time.

5. Conclusions

The study that was carried out has given new insights into the formation of GSR and its analysis. The use of a FEG-SEM with an *X-flash* flat quad detector has allowed for in depth particle analysis of a higher spatial resolution at sub-micron magnifications. This, in turn, has led to a deeper understanding of particle morphology, showcasing new impact disrupted GSR structures that were previously unknown. Similarly, the ability to determine the elemental composition of specific features within particles measuring less than 1 μm in diameter, creates new possibilities into the standard of GSR analyses. This information may have a great implication on the automated analysis of GSR in laboratories and law agencies. Particles collected that may have previously been discarded due to their

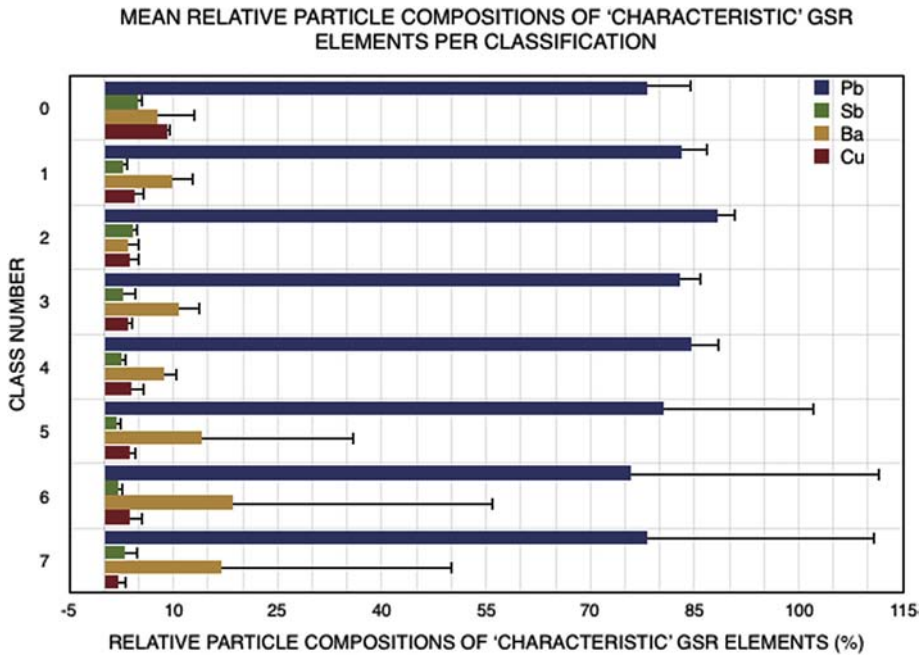

Fig. 8. Figure displaying the averages of the relative proportions of 'characteristic' GSR elements ± 1 standard deviation.

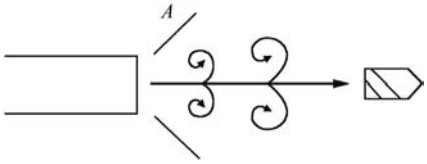

Fig. 9. Figure showing the firearm discharge plume expansion as a projectile leaves the firearm.

lack of all three 'characteristic' GSR elements may in fact be a segment of a greater splat structure, leading to the re-evaluation of sample collection protocols and analysis world wide.

Acknowledgements

The author would like to thank Dr Mark Price for his vital support and encouragement during this process as well as Mr Mark Johnson for his time and resource contribution to this experiment.

This research did not receive any specific grant from funding agencies in the public, commercial, or not-for-profit sectors.

References

[1] Schwoeble AJ, Exline DL. Current methods in forensic gunshot residue analysis. Boca Raton, London, New York, Washington D.C: CRC Press; 2000.
[2] Wallace JS. Chemical analysis of firearms, ammunition and gunshot residue. CRC Press; 2008.
[3] Dalby O, Butler D, Birkett JW. Analysis of gunshot residue and associated materials - a review. J Forensic Sci 2010;55:924–43.
[4] ASTM E1588–10e1. Standard guide for GSR analysis by scanning electron microscopy/energy dispersive X-ray spectrometry. West Conshohocken, PA: American Society for Testing and Materials; 2010.
[5] Brożek - Mucha Z. Chemical and morphological study of gunshot residue persisting on the shooter by means of scanning electron microscopy and energy dispersive X-ray spectrometry. Microsc Microanal 2011;17(6):972–82.
[6] Steffen S, Otto M, Niewoehner L, Barth M, Brożek - Mucha Z, Biegstraaten J, Horvath R. Chemometric classification of gunshot residue based on energy dispersive X-ray microanalysis and inductively coupled plasma analysis with mass-spectrometric detection. Spectrochim Acta B 2007;62:1028–36.
[7] Wolten GM, Nesbitt RS, Calloway AR, Loper GL. Particle analysis for the detection of gunshot residue II: occupational and environmental particles. J Forensic Sci 1979;24(2):423–30.
[8] Mosher PV, McVicar MJ, Randall ED, Sild EH. Gunshot residue-similar particles produced by fireworks. J Can Soc Forensic Sci 1998;31(3):157–68.
[9] Cardinetti B, Ciampini C, D'Onofrio C, Orlando G, Gravina L, Ferrari F, Di Tullio D, Torresi L. X-ray mapping technique: a preliminary study in discriminating gunshot residue particles from aggregates of environmental occupational origin. Forensic Sci Int 2004;143(1):1–19.
[10] Garofano L, Capra M, Ferrari F, Bizzaro GP, Di Tullio D, Dell'Olio M, Ghitti A. Gunshot residue. Further studies on particles of environmental and occupational origin. Forensic Sci Int 1999;103(1):1–21.
[11] Ilker Kara, Yasin Sarikavakc, Sefer Bora Lisesivdinb, Mehmet Kasapb. Evaluation of morphological and chemical differences of gunshot residues in different ammunitions using SEM/EDS technique. Environ Forensics 2016;17(1):68–79.
[12] Basu S. Formation of gunshot residues. J Forensic Sci JFSCA 1982;27(1):72–91.
[13] Aoudjehane H. C. et al, Tissint Martian Meteorite: a fresh look at the interior, surface and atmosphere of Mars, Science, Vol. 338, 6108, 785–788
[14] Goldstein J, Newbury D, Joy D, Lyman C, Echlin P, Lifshin E, Sawyer L, Michael J. Scanning electron microscopy and X-ray microanalysis. 3rd ed. Springer; 2003.
[15] Firearm Examiner Guide. http://projects.nfstc.org/firearms/module12/fir_m12_t05_03_j.htm. last accessed December 2016.